
Development and energy evaluation of novel integrated envelopes without thermal bridges

Ru Ji^{a*}, Yaxian Zheng^a, Ziwei Chen^b, Shen Wei^c

^a School of Civil and Resource Engineering, University of Science and Technology Beijing, 100083, Beijing, P.R. China

^b Department of Energy and Resources Engineering, College of Engineering, Peking University, 100871 Beijing, PR China

^c The Bartlett School of Construction and Project Management, University College London (UCL), 1-19 Torrington Place, London WC1E 7HB, United Kingdom

*Corresponding author: jiru@ustb.edu.cn

Abstract

In this study, to eliminate thermal bridges caused by traditional insulation system, a new synthesis method of novel integrated envelopes was proposed. This proposed integrated envelope consisted of two layers, including the base part and insulation part. Construction solid wastes were applied as raw materials and the influences of the raw material ratio, additive content, and sintering temperature on micro and macro performances were investigated. The experiment results show that the optimal sample was sintered at 1200°C, with raw materials of 50wt.% waste glass, 40wt.% mineral wool waste, 10wt.% waste quartz for both parts, and with another 2wt.% SiC and 1~3wt.% Na₃PO₄·12H₂O for the insulation part. The corresponding optimal samples have the best performance, such as the dense base, a uniform pore structure, and good thermal insulation. Moreover, the energy analysis results revealed that this proposed material has good environmental sustainability and could efficiently reduce the negative impact of thermal bridges with the energy conservation of 8.18%.

Keywords:

Integrated envelope; building energy-saving; thermal bridges; construction solid waste.

Introduction

China's urbanization is developing rapidly, making the construction industry account for 26.7% of the entire GDP [1-2]. The biggest phenomenon is the continuous increase in building area, according to the survey in 2015 the total building area including buildings under construction and completed was up to 16.4 billion square meters [3]. These increasing number of buildings lead to two kinds of challenges, including the construction solid waste (CSW) and building energy consumption.

As an issue of big amount of buildings increasing, building energy consumption has reached high up to 40% of the total energy use of the whole society [4]. High thermal insulation materials are an excellent method to solve this problem [5]. For example, wool fiber and foam ceramics, as one of the inorganic insulation materials, have attracted lots of attention and been widely applied in buildings due to its excellent properties, including low density, high specific strength, and low thermal conductivity [6-7]. However, there is a problem need to be noted, which is the fixing problem of the traditional insulation board. Anchor bolts, as a common anchoring method, would exert negative effects on thermal insulation performance, due to its high thermal conductivity [8]. In addition, when anchoring, it also causes the insulation system to rupture sometimes. Therefore, a novel insulation material without thermal bridges caused by the fixing issue is further required.

As another big issue, CSW continues to grow in recent decades and has caused environment pollution growth without reasonable handling [9]. Construction solid waste (CSW) activities are a major source of waste; their share varies between 13% and 40%

of the total solid waste generated, depending on the country. It is estimated that about 30%~46% of CSW generated is recycled in the world [10-11]. According to the literature [12], in China, 2 billion tons of CSW is produced each year, accounting for more than 30% of the municipal solid waste. Waste glass (WG) is a main CSW, and there is a sustained growth in the quantities of waste glass [13]. In China, the annual generation of WG is more than 40 million tons [14], while only parts of WG is utilized for preparing building materials, such as stoneware tile and concrete [15-19]. Actually, large amounts of WG ends up in landfills [20]. Mineral wool waste (MW) is a generated as both process waste from mineral wool production and solid waste from the CSW industry [21]. According to the survey [22], the generation of MW accounts to about 0.3% CSW. Several previous studies have carried out to propose the reuse method for MW, and it can be concluded to two major alternative methods. One is to reuse MW into its preparation process [23], and the other one is to use it as a raw material in the synthesis of other construction materials [24]. However, these two methods both present some restrictions on substantial mineral wool waste recovery, including causing the equipment clogging and the limited reuse amount of MW for above recycling methods. Consequently, until now there is a large amount of MW disposed of, which leads to environmental problems [25]. In addition, waste quartz (WQ) is one of the industrial chemical wastes [26-27]. In WQ, the SiO₂ content can exceed 80%, and it often consists of metal oxides, such as CaO, Al₂O₃, K₂O, and Na₂O [28]. The composition of WQ makes it often used in the preparation of inorganic materials such as glass ceramics [29].

In conclusion, to eliminate thermal bridges by traditional insulation system, this study was proposed to synthesize novel integrated envelopes. And due to the composition of MW, WG, and WQ are have the similarity with traditional ceramic preparation raw materials, they were collected as raw materials of this integrated

envelope material. It is needed to note that this proposed integrated envelope material consists of two parts, named as the base layer and the insulation layer, which can make it have high insulation performance without the fixing problem. In this study, the effects of the raw material ratio, sintering conditions such as additive contents and sintering temperatures on micro and macro-properties of sintered samples were investigated systematically. Finally, an energy evaluation of this proposed material, including environmental sustainability and operation energy reduction, would be given.

2. Experimental procedure

2.1 Raw materials

To prepare the integrated envelope, two parts, named as the base layer and the insulation layer, needed to be studied, so there were two kinds of raw material compositions for the sample synthesis. For the base layer, its raw materials were composed of waste quartz (WQ), mineral wool waste (MW), and waste glass (WG). Here, mineral wool and waste quartz were collected from Shanxi province, China, and waste glass was recycled from municipal construction solid waste. For the insulation layer, the same raw materials would be applied, but silicon carbide powder (SiC) with a mean particle size of 55 μ m would be used as a foaming agent because it emits gas as described in the literature [30]. Moreover, sodium phosphate ($\text{Na}_3\text{PO}_4 \cdot 12\text{H}_2\text{O}$) was selected as a foam stabilizer as well as fluxing agent based on the different role of its decomposition products of Na_2O and P_2O_5 . Specifically, P_2O_5 could prevent the pores from bursting or interconnecting by increasing the viscosity of the glass melt at high temperature, so $\text{Na}_3\text{PO}_4 \cdot 12\text{H}_2\text{O}$ was employed to stabilize the pore structure.

Before sintering, the chemical compositions and crystalline phase of these raw materials were analyzed by XRF and XRD tests and the measurement results were shown in Table 1 and Figure 1. XRF data in Table 1 shows that the main chemical

constituents of mineral wool waste are SiO_2 and Al_2O_3 , while waste glass and waste quartz mainly contain SiO_2 . XRD data in Figure 1 indicates that mineral wool waste and waste glass are both amorphous, and the major crystalline phase in waste quartz is quartz.

Table 1: The chemical compositions of raw materials (wt.%)

Materials	SiO_2	Al_2O_3	TiO_2	Fe_2O_3	CaO	K_2O	MgO	Na_2O	SO_3	LOI
Mineral wool waste	52.56	42.27	0.81	3.32	0.36	0.27	0.09	0.09	0.02	0.01
Waste glass	72.25	1.10	0.03	0.97	9.25	0.40	3.70	12.00	0.18	0.04
Waste quartz	96.50	0.63	0.03	0.30	1.40	0.23	0.10	0.04	0.03	0.07

*LOI (loss on ignition)

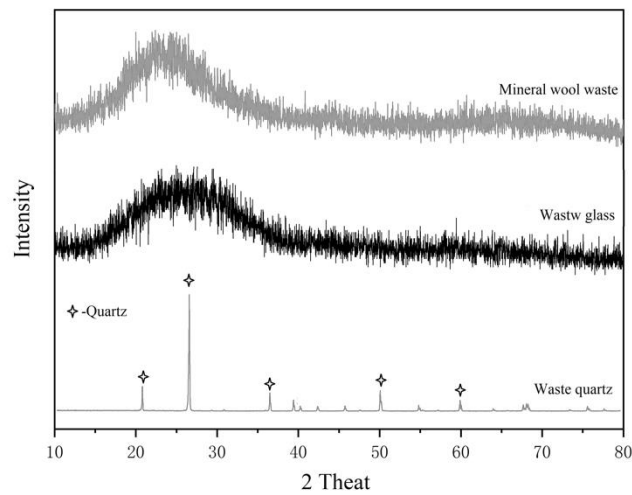


Figure 1: XRD pattern of raw materials

2.2 Sample preparation

In this study, for both layers, the compositions of green samples were prepared by mixing raw materials in different mass ratios from 3:6:1 to 7:2:1 (waste glass: mineral wool waste: waste quartz). While for insulation layer, different silicon carbide addition of 0~4wt.% was be further added in green samples. As shown in Table 2, the corresponding samples were named as B1 to B5 and I1 to I5, for the base layer and the insulation layer, respectively.

Table 2: Main raw materials compositions of green samples (wt.%)

Sample	Waste glass	Mineral wool waste	Waste quartz
B1/I1	30	60	10
B2/I2	40	50	10
B3/I3	50	40	10
B4/I4	60	30	10
B5/I5	70	20	10

Here, three kinds of main raw materials, MW, WQ, and WG, were separately dry ball-milled using a planetary ball mill machine for 2h, then the powder was sieved through a 200 meshes sieve. Then, according to the designed raw material proportion in Table 2, all of the raw materials including SiC were ground in mill jars with a planetary ball mill for 8hours. Next, the polyvinyl alcohol solution was added to the powder mixtures as a binder. Finally, the green sample disks with a diameter of 22mm and thickness of 10mm were prepared by using a pressure of 15MPa added to powder mixtures.

Then, the green disk samples were initially heated at 600°C for 40min in a muffle furnace in order to remove water trapped in samples and to keep samples in equal heat distribution. Afterward, the samples were heated to a peak temperature from 800°C to 1300°C at a heating rate of 20°C/min a hold of 20min at the peak temperature. Finally, the stinted samples were naturally cooled to room temperature in a muffle furnace.

2.3 Characterization techniques

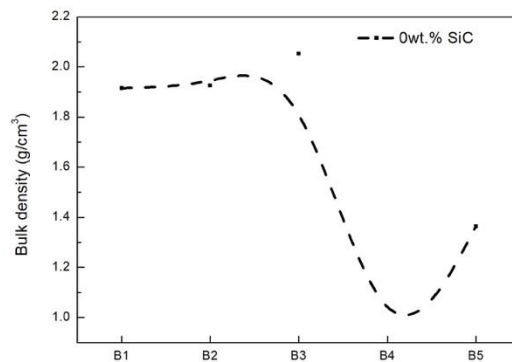
Bulk density of stinted samples was determined either by measuring the weight and the volume by using the Archimedes method or directly testing its external size. The crystalline phases were analyzed by X-ray diffraction (Rigaku D/max 2550PC X-ray using Cu K α radiation, a scanning rate of 8°/min over a scanning range of 10-80°). Microstructure observations of matrix structure and internal pores of stinted samples were investigated using Scanning electron microscope (SEM).

3. Results and discussion

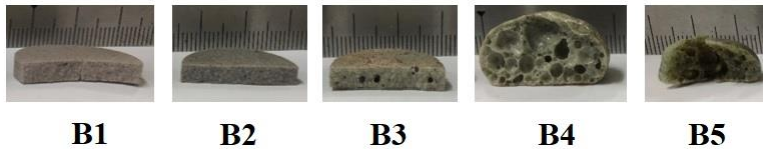
3.1 The study of influence parameters

3.1.1 Raw material composition

For the base part, Figure 2 indicates the bulk density variation and appearance sectional view of samples B1~B5 with no formed agent of SiC sintered at 1200°C. First, Figure 2a shows that, for samples from B1 to B3, bulk density keep in a peaceful area; while for samples B3 to B4, bulk density rapidly decreases from 2.05g/cm³ to 0.71g/cm³; then for samples from B4 to B5, a rise of bulk density from 0.71g/cm³ to 1.36g/cm³ occurs. Meanwhile, Figure 2b shows the consistently corresponding volume change from B1 to B5, i.e. the sample volume of B4 is the biggest, then it decreases for sample B5. This evolution can be explained as follow.



(a) Variations of bulk density



(b) A sectional view

Figure 2: Variation of bulk density and a sectional view of base part samples without SiC at 1200°C

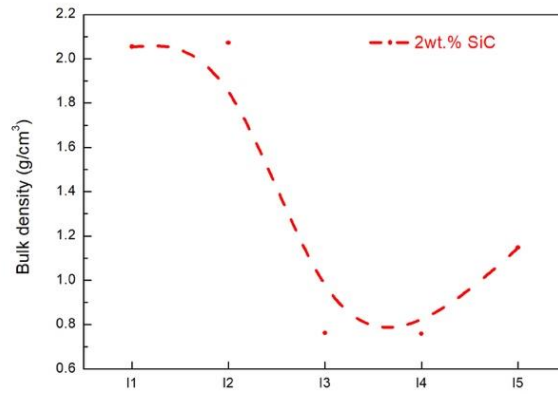
Before sintered samples B1 to B5, the bulk density of the green sample was tested, and a bulk density of 1.37 g/cm³ was got. For samples B1 to B3, it can be concluded that compared to the green sample, there is a big rise of bulk density, which is attributed to

the densification of the internal structure of the sintered sample, caused by high-temperature sintering. Here, the increasing densification resulted in the denser base of samples, which could be selected as a base part in the synthesis of an integrated envelope.

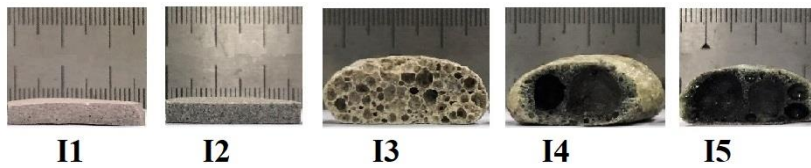
Then for the sample B4, it is interesting to note that even though in the sample B4 no SiC added, it still could be observed that the foaming phenomenon occurs at this high sintering temperature of 1200°C. This is attributed to the chemical reaction of the ferric oxide (Fe₂O₃), which could be detected in the mineral wool waste in the raw materials. Here, Fe₂O₃ acted as a foaming agent and released O₂ according to Equation (1) [31]. At the same time, for the sample B4, more waste glass (60wt.%) was added into the raw materials, leading to more liquefaction further generated in the body, which would be good for the remaining of pores caused by O₂ gas. Consequently, the sample B4 has a low bulk density. However, from the sectional view in Figure2b, it can also be seen that the pores in sample 4 are extremely uneven and very large, which is bad for its mechanical and thermal insulation properties.



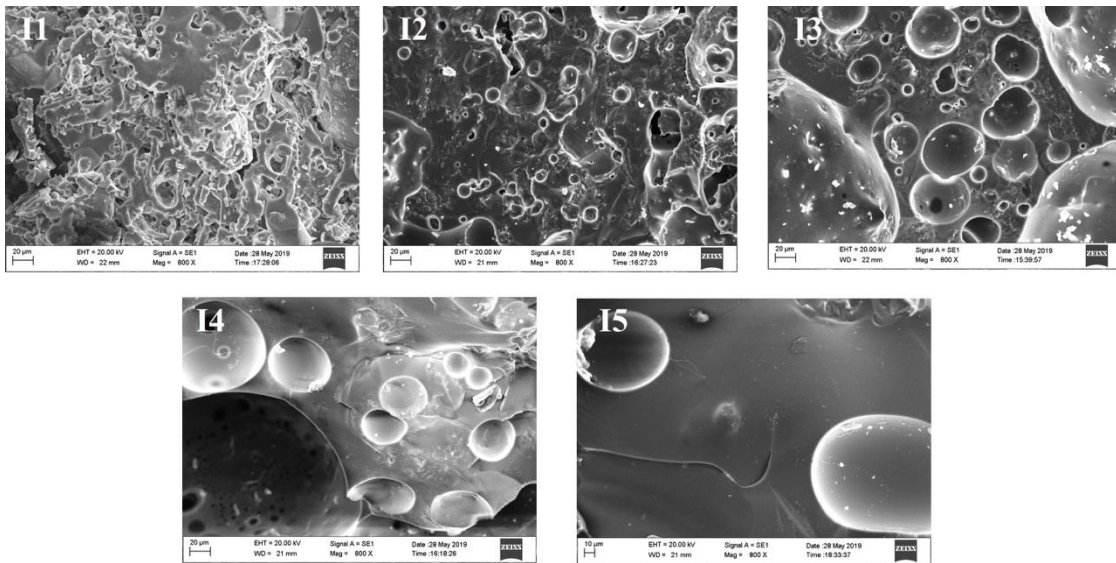
Finally, for the sample B5, with the further increase of waste glass addition, the liquefaction phenomenon would further be intensified, which resulted in the matrix viscosity of the sample B5 extremely reduced. As a result, the generated gases in the sample B5 are further concentrated and overflow from the surface, eventually resulting in a slight increase in bulk density.



(a) Variations of bulk density



(b) A sectional view



(c) SEM

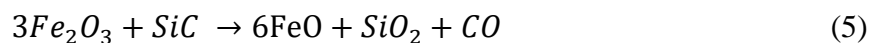
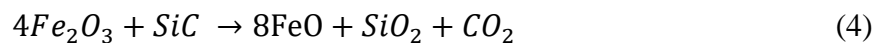
Figure 3: Variation of bulk density, a sectional view picture and SEM of insulation part samples with 2wt.% SiC at 1200°C

For the insulation part, Figure 3 shows the bulk density variation, appearance sectional view, and SEM image of samples I1~I5 with 2wt.% SiC sintered at 1200°C. Figure 3 also shows similar trends compared with the curves in Figure 2. Specifically, in Figure 3a, for samples from I1 to I5, bulk density firstly decreases, then increases slightly. Meanwhile, the corresponding volume changes consistently as shown in Figure

3b. Moreover, SEM image could indicate the detail change in these samples. Specifically, the matrix of samples become more and more densification with the increase of waste glass. For the sample I3, there is the obvious generation of pores in the sample body due to the gas formed, and which are evenly distributed. While with the further increase of waste glass, the small pores gather into big pores, and even disappear in the sample body, leading to the decrease of the sample volume and the increase of the bulk density. It can be concluded that, these changes in samples' body are consistent with that in their macro properties, such as the bulk density and volume.

It is interesting to note that, there are some differences in samples between the insulation part and the base part. First, among insulation part samples, the pore generation appeared in advance in the sample I3 with 50wt.% waste glass addition, compared with the phenomenon among base part samples. Moreover, as can be seen from the cross-sectional view in Figure3b, the pores in Sample I3 are more evenly distributed and there are no oversized pores that affect its macro performance. The sample I3, therefore, could be selected to synthesize the insulation part of the integrated envelope.

Here, the gas generation is mainly due to the reaction of silicon carbide powder (SiC), which emits gas as indicated by Equations (2) and (3) [30]. In addition, for insulation part samples containing SiC addition, Fe₂O₃ from mineral wool waste, as a source of O₂ (based on Equation (1)), could promote gas generating cooperating with SiC described as Equation (4) and (5) [31].



In conclusion, for base part samples, an increasing content of waste glass would promote the body sintering, leading to the formation of a liquefied body at a set high sintering temperature, which can contribute to the increase of its body strength. However, an over added of waste glass will also resulted in the gas formation in the sample body, which is bad for its overall strength. An appropriate raw materials ratio B3 is necessary for the synthesis of the base part sample. Moreover, for insulation part samples, a suitable ratio of the raw materials would also make the sample body have an appropriate degree of the liquefaction, which can further effectively maintain the gas released by the foaming agent in the body. Then the insulation part samples would have pores of appropriate size and uniform distribution, facilitating its dual performance of mechanical and thermal insulation. In summary, in this study the samples B3 and I3 with 50wt.% waste glass meet the requirements of the above two partial samples and are therefore selected for subsequent experiments.

3.1.2 Sintering temperatures

The choice of sintering temperature is critical to the overall performance of the integrated material. In this study, in order to prepare an integrated energy-saving envelope material, it is necessary to carry out one-time sintering process of the two-layer samples at the same temperature, so the sintering temperature must simultaneously make the two-layer samples have the best performance. That is, the base layer has a high density, the insulation layer has a good pore structure. Since silicon carbide was used as a foaming agent for the insulation layer in this study, the sintering temperature must be in the high temperature range of about 1100°C to 1300°C. Finally, the sintering temperature is selected depending on the selection of the raw materials and the specific sintering effect.

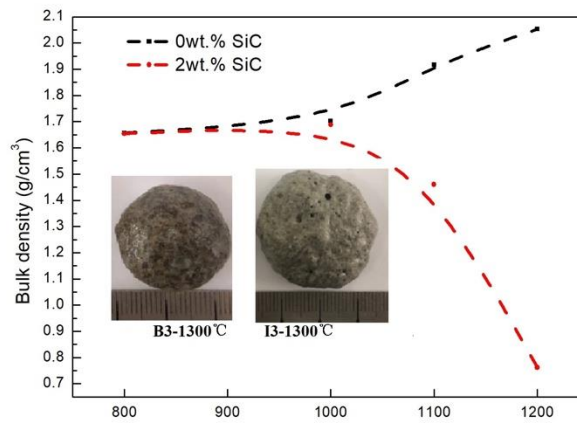


Figure 4: Variation of bulk density of sintered samples B3 and I3 at different temperatures

Figure 4 indicated the bulk density variation of samples B3 and I3 under the effect of sintering temperatures. As shown in Figure 4, the densities of samples B3 increase as the sintering temperature increased, while for samples I3 it decreases instead. Specifically, the sample B3 sintered at 800°C has the minimum bulk density of 1.66 g/cm³, then at 1200°C it increases up to 2.05 g/cm³, with a growth rate of 23.5%; while sintered sample I3 at 800°C exists the maximum bulk density of 1.65 g/cm³, then it slightly reduces to 1.46 g/cm³ at 1100°C, finally it sharply decreases to 0.76 g/cm³ at 1200°C.

Next, a detailed analysis of the effect of sintering temperatures will be carried out. For base part samples, an increase in bulk density exists as sintering temperature increases. This is due to a rise in sintering temperatures, which would benefit the body's liquefaction, thus leading to an increase of sample's bulk density. For insulation part samples, when the sintering temperatures are above 1000°C, a different process existed in samples I3 compared with base part samples B3. In samples I3, the liquid phase would also continually accelerates with the increase of sintering temperature, resulting in the promotion of the liquefaction and the matrix densification of samples I3. While, at the

same time, at high sintering temperatures, the foaming agent SiC would decompose and release CO₂/CO gas. Consequently, increased liquid phase generation is a benefit to retaining the generated gas by SiC in the sample body, then pores occur in the sample I3. Next, the pores lower the bulk density of the sample I3.

Actually, higher sintering temperatures (over 1200°C) was set to synthesize both part samples, but it would get the bad results. This is because that when the sintering temperature further increases, like 1300°C, in both bodies of base and insulation part samples, both the body liquefaction and gas generations (caused by Fe₂O₃ and SiC respectively) accelerate significantly. Then, small pores aggregate into larger pores and even spill from sample surfaces, resulting in the irregular deformation of samples. Therefore, samples B3 and I3 sintered at 1200°C have better performances.

3.1.3 Foaming agents

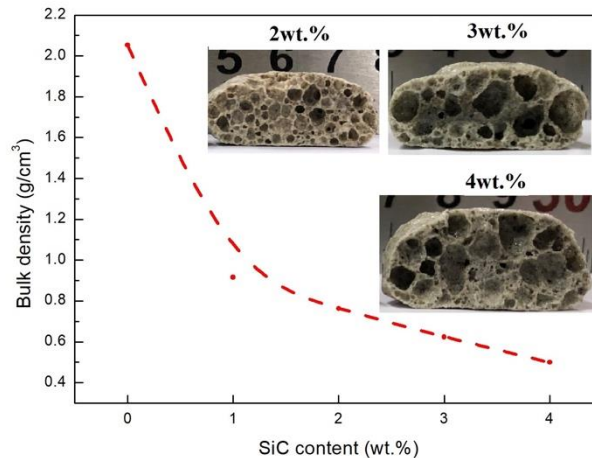


Figure 5: Bulk density variation of samples I3 with the different foaming agent

Figure 5 gives the bulk density variation of sample I3 under the effect of different foaming agents, there is a dropping trend with the increase of SiC. First, with an increasing foaming agent content from 0wt.% to 1wt.%, sample bulk density decreases drastically from 2.05 g/cm³ to 0.92 g/cm³, with a reduced rate of 55%. This is due to the function of both the liquefaction and the foaming phenomenon in the sample I3 body.

Specifically, in the sample without SiC addition, there is only the liquefaction in the body, while in the sample with 1wt.% SiC, in addition to liquefaction, there is also a generation of foaming, so the bulk density drops sharply. Secondly, with the further increasing SiC addition, bulk density further reduces slowly, from 0.92 g/cm³ to 0.50 g/cm³ for added foaming agent from 1wt.% to 4wt.%. However, from the sectional view of samples I3 with different SiC addition, when the content of the foaming agent exceeds 2wt.%, the size of the pores sharply increases and the distribution becomes uneven. Consequently 2wt.% SiC addition of foaming agent is appropriate for the preparing of insulation part sample.

3.1.4 Additives of sodium phosphate

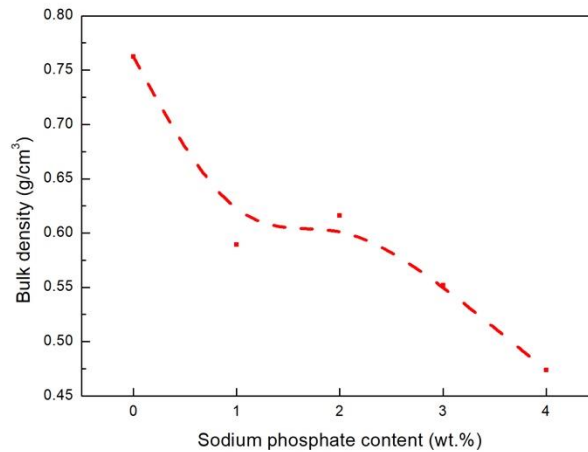


Figure 6: Bulk density variation of samples I3 with different sodium phosphate

In this section, for improving the pore structure, sodium phosphate as foam stabilizer was added to samples I3. And its bulk density and cross-sectional microstructure were carried out to indicate the effect of sodium phosphate, as shown in Figure 6 and 7.

First, it can be found that from Figure 7, compared with the sample I3 without Na₃PO₄·12H₂O, more rounded pores are detected in samples I3 with Na₃PO₄·12H₂O adding, which would strengthen the mechanical behavior of samples. This optimization

of pore structures is due to the generation of P_2O_5 decomposed by sodium phosphate, which can stabilize the formation of pores.

Secondly, Figure 6 shows that as the amount of stabilizer $Na_3PO_4 \cdot 12H_2O$ added increases, the bulk density becomes smaller. In particular, for samples with 0wt.% and 1wt.% $Na_3PO_4 \cdot 12H_2O$ addition, a relatively big drop in bulk density exists, which are 0.76 g/cm^3 and 0.59 g/cm^3 respectively, with a decline rate of 22.4%. It can be explained that $Na_3PO_4 \cdot 12H_2O$ would also promote the body liquefaction of samples due to an existence of Na_2O as another decomposition product by $Na_3PO_4 \cdot 12H_2O$, which is a benefit to the bubble growth. The corresponding consistent phenomenon could be also seen in Figure 7, i.e. the matrix becomes more densification and pore structures become larger with the increase of $Na_3PO_4 \cdot 12H_2O$ addition. However, it should be noted that excessive $Na_3PO_4 \cdot 12H_2O$ add could make more small pores tend to bigger, and may escape from the sample surface, which would be bad for the sample's performance.

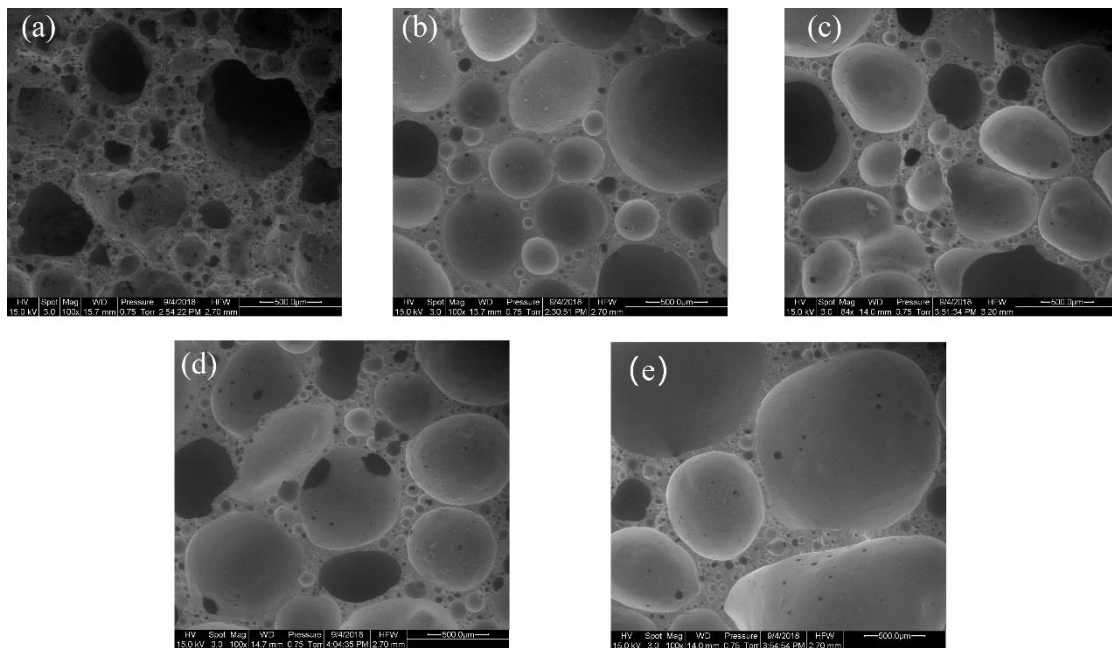


Figure 7: The cross-sectional microstructure of samples I3 with different sodium phosphate (a) 0wt.%, (b) 1wt.%, (c) 2wt.%, (d) 3wt.%, (e)4 wt.%

3.2 Synthesis of the integrated envelope and its energy evaluation

3.2.1 Synthesis of the integrated envelope

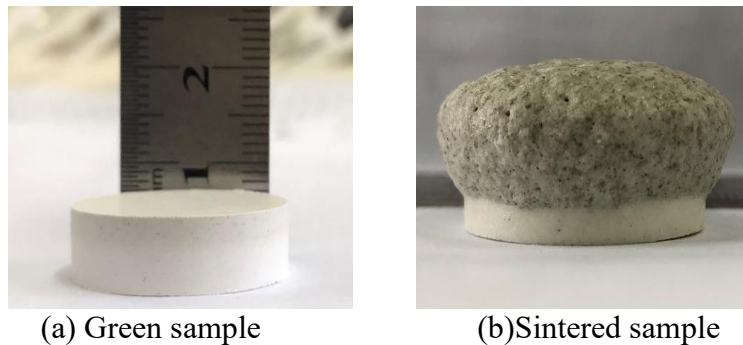


Figure 8: The green sample and the sintered sample of the integrated envelope with both parts B3/I3

According to the experiment results above, the sample B3 and the sample I3 were applied for the preparation of the integrated envelope by sintering at 1200°C. In this study, at first separately mixed these two groups of raw materials as shown in Table 2, then put the two mixed powders in the model separately, and next pressed them together into a green sample under 5 MPa (Figure 8a), finally got sintered integrated envelopes after sintering in a furnace (Figure 8b). Figure 8b shows that there are two parts in this sintered sample, namely the base part and the insulation part, but they just fit together. To further investigate the combination of the two parts, an SEM image of the sectional view for this integrated envelope was detected as shown in Figure 9. This microstructure image indicates that the combination of the two parts is excellent, and there is no crack between them, which contributes to the integral structure. This good combination is mainly due to the fact that the two parts of the raw materials are pressed together, and the raw material compositions are consistent except for the foaming agent. Thus the matrix of two parts have the same degree of liquefaction at the time of high-temperature sintering and can be perfectly matched. It is, therefore, acceptable to prepare an integrated envelope in this proposed method.

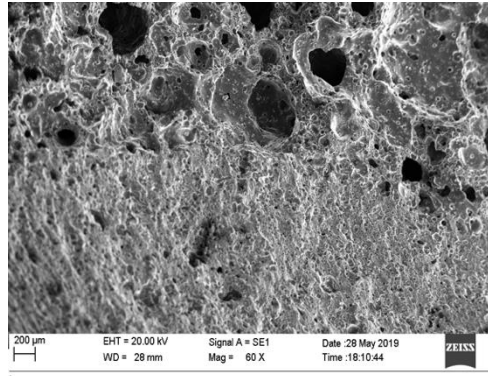


Figure 9: SEM image of the sectional view for this integrated envelope

3.2.2 Environmental sustainability analysis

In this part, the environmental sustainability of this proposed material was evaluated by using SUB-RAW index by Bontempi E [32]. Here, SUB-RAW index is a new simple approach based on the use of two environmental indicators embodied energy (EE) and CO₂ footprint (CF). Embodied energy (EE) is the energy utilized during the manufacturing stage of products and represents the energy used to acquire raw materials (excavation), manufacture and transport. Similarly, CO₂ footprint (CF) is evaluated from environmental indicators which represent the equivalent emissions for products within the LCA boundary [33].

The SUB-RAW index can be calculated by taking the corresponding EE and CF values (Table 2) into the Equation 1 [34-36]. Then it can be assessed the environmental sustainability of the newly proposed material in this paper, here the positive value of this index indicates the increased sustainability of a newly proposed material compared to the raw material to be substituted [32].

$$\text{SUB - RAW index} = [\log(\text{EE}_{\text{raw}}/(\text{MJ}/\text{kg})) - \log(\text{EE}_{\text{sub}}/(\text{MJ}/\text{kg})) + \log(\text{CF}_{\text{raw}}) - \log(\text{CF}_{\text{sub}})]/2 \quad (1)$$

Where, EE_{raw} is the embodied energy of the raw material in MJ/kg; EE_{sub} is the embodied energy of the newly proposed material in MJ/kg; CF_{raw} is the CO₂ footprint of the raw material in kg/kg; CF_{sub} is the CO₂ footprint of the newly proposed material in kg/kg.

Here, it is needed to note that, the raw materials used in the traditional ceramic wall product contain clay, quartz and feldspar, while in this study the raw materials were all from construction solid waste. According to the literature [37], the embodied energy of waste material can be considered as zero, compared with the natural raw materials and manufactured products, then the EE and CF of the proposed material can be got as shown in Table 2.

Table 3: the embodied energy and CO₂ footprint values of the materials involved

Materials	Embodied energy (MJ/kg)	CO ₂ footprint (kg/kg)
Clay	4.30	0.24
Quartz	0.85	0.02
Feldspar	1.30	0.20
Ceramic wall product	9.00	0.59
Proposed material	6.59	0.31

Then we could get the SUB- RAW index value (0.21) of our proposed material, which indicated the increased sustainability, depicting that the newly proposed material behaved the more environmental sustainability than that of traditional ceramic wall product.

3.2.3 Operation energy analysis

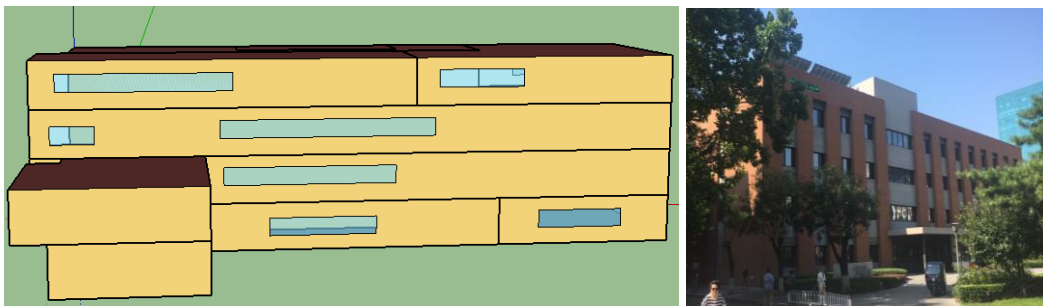
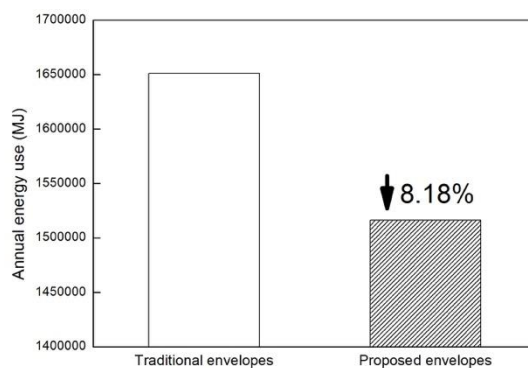


Figure 10: The building model for evaluating the energy performance of the integrated envelope

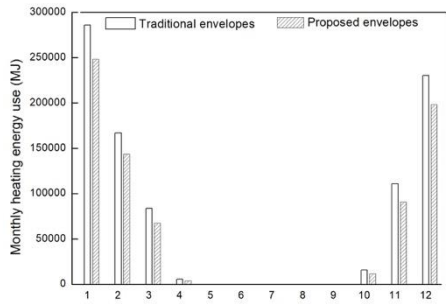
Moreover, the building energy-saving performance of this proposed integrated envelopes will be testified by using EnergyPlus software. In this simulation, conduction transfer function was applied as the heat balance algorithm and the time discretization

for calculation is 15min. Specifically, a real building in Beijing was used as a reference for this simulation, and the simulation model with 4 floors built by EnergyPlus was shown in Figure 10. To run this simulation model, an ideal load HVAC system was used to control its indoor air temperature, which was kept between 18°C and 26°C. In addition, to get an accurate energy analysis of the proposed envelopes, interior heat source, such as lights, electric equipment, people, was considered as the real functional zones of the building.

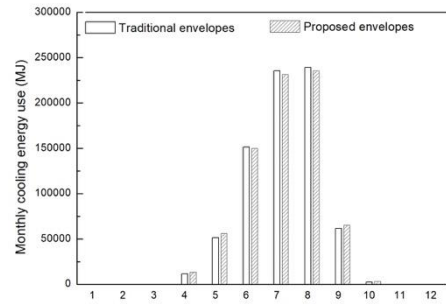
In this simulation, two kinds of external envelopes were applied, including the traditional envelope acting as basement group and the proposed envelope with the integrated envelope. Specifically, for the traditional envelope, two layers are 190mm reinforced concrete and 35mm mineral wool board with anchors fixed, and the corresponding thermal conductivities are 0.077 W/(m·K) and 1.950 W/(m·K), respectively. Here, it is needed to note that, the thermal conductivity of mineral wool is 0.048 W/(m·K), but its effective value is increased due to the added of metal anchors. While for the proposed envelope, two layers are consist of by the integrated envelope, which are 190mm base part (B3) and 35mm insulation part (I3), with thermal conductivities of 0.130 W/(m·K) and 0.411 W/(m·K), respectively.



(a) Annual energy use



(b) Monthly heating energy use.



(c) Monthly cooling energy use

Figure 11: Annual and monthly energy use for different building envelopes

Figure 11 indicates annual and monthly energy use for these two kinds of building envelopes. Figure 11a shows that the annual energy use is efficiently reduced by $1.35E+5$ MJ and a decrease of 8.18% when replacing the traditional envelope with this proposed integrated envelope. Thus, if this integrated envelope could be used in other buildings in China, the energy-saving would be remarkable.

Moreover, it can be seen from Figure 11b and c, the reduction of energy use is mainly due to the contribution of heating energy use in winter, which means that the use of integrated envelope can prevent the side effects caused by the anchors of traditional thermal insulation system, resulting in the improvement of the insulation performance of buildings.

4. Conclusion

In this study, a novel integrated envelope was synthesized by using construction solid waste, and the main results are shown as following.

- In the synthesis of two parts samples, both raw material composition and sintering conditions have a significant influence on samples' micro and macro performances.
- For both parts, main raw material compositions are 50wt.% waste glass, 40wt.% mineral wool waste, and 10wt.% waste quartz, while in insulation part the

additives of 2wt.% SiC and 1~3wt.% Na₃PO₄·12H₂O are further needed, sintered at 1200°C.

- The synthesized integrated envelope could be got by one-time sintering process, and it has excellent properties, such as bulk densities of 2.05g/cm³ and 0.76g/cm³ and thermal conductivities of 0.411W/(m·K) and 0.130W/(m·K), for base part and insulation part, respectively.
- The energy analysis results show that this proposed material could get positive SUB- RAW index value, depicting its environmental sustainability, and it could efficiently prevent thermal bridges caused by the anchors, and reduce the energy use of buildings by about 8.18%.

Acknowledgments

This paper was supported by the National Natural Science Foundation of China (51708022). Supports by The Fundamental Research Funds for the Central Universities (FRF-TP-18-024A2), Student Research Training Program in China, and the program of China Scholarships Council (201806465006) are also acknowledged.

References

- [1]. Zheng L, Wu H, Zhang H, et al. Characterizing the generation and flows of construction and demolition waste in China [J]. *Construction and Building Materials*, 2017, 136:405-413
- [2]. Shi J, Lin K W, Chen Z Q, et al. Annual Dynamic Thermal Performance of Solar Water Heaters: A Case Study in China's Jiangsu Province [J]. *Energy and Buildings*, 2018, 173.
- [3]. National Bureau of Statistics of the People's Republic of China (NBSC), 2002–2016a. *China City Statistical Yearbook*.

-
- [4]. Sartori I , Sandberg N H , Bratteb? H . Dynamic building stock modelling: General algorithm and exemplification for Norway[J]. *Energy and Buildings*, 2016:S037877881630487X
- [5]. Ji R , Wu S , Yan C , et al. Preparation and characterization of the one-piece wall ceramic board by using solid wastes[J]. *Ceramics International*, 2017:S0272884217304625.
- [6]. Berardi U, Naldi M. The impact of the temperature dependent thermal conductivity of insulating materials on the effective building envelope performance[J]. *Energy & Buildings*, 2017, 144:262-275.
- [7]. Zhu M , Ji R , Li Z , et al. Preparation of glass ceramic foams for thermal insulation applications from coal fly ash and waste glass[J]. *Construction and Building Materials*, 2016, 112:398-405.
- [8]. Ji R, Zhang Z, He Y, et al. Simulating the effects of anchors on the thermal performance of building insulation systems[J]. *Energy & Buildings*, 2017, 140:501-507.
- [9]. Jiménez J R, Ayuso J, López M, et al. Use of fine recycled aggregates from ceramic waste in masonry mortar manufacturing[J]. *Construction & Building Materials*, 2013, 40(3):679-690.
- [10]. Galan B, Dosal E, Andrés A, et al. Optimisation of the construction and demolition waste management facilities location in Cantabria (Spain) under economical and environmental criteria[J]. *Waste & Biomass Valorization*, 2013, 4(4):797-808.
- [11]. Yuan H, Shen L . Trend of the research on construction and demolition waste management[J]. *Waste Manag*, 2011, 31(4):670-679.
- [12]. Tam, V., & Lu, W. Construction waste management profiles, practices, and performance: a cross-jurisdictional analysis in four countries[J]. *Sustainability*, 2016, 8(2), 190.

-
- [13]. Bernardo E, Bonomo E, Dattoli A. Optimisation of sintered glass–ceramics from an industrial waste glass[J]. *Ceramics International*, 2010, 36(5):1675-1680.
- [14]. Mao R , Duan H , Gao H , et al. Characterizing the Generation and Management of a New Construction Waste in China: Glass Curtain Wall[J]. *Procedia Environmental Sciences*, 2016, 31:204-210.
- [15]. Luz A P, Ribeiro S. Use of glass waste as a raw material in porcelain stoneware tile mixtures[J]. *Ceramics International*, 2007, 33(5):761-765.
- [16]. Rambaldi E, Carty W M, Tucci A, et al. Using waste glass as a partial flux substitution and pyroplastic deformation of a porcelain stoneware tile body[J]. *Ceramics International*, 2007, 33(5):727-733.
- [17]. Spiesz P, Rouvas S, Brouwers H J H. Utilization of waste glass in translucent and photocatalytic concrete[J]. *Construction & Building Materials*, 2016, 128:436-448.
- [18]. Sun K I, Yeong C S, Ik Y E. Evaluation of durability of concrete substituted heavyweight waste glass as fine aggregate[J]. *Construction and Building Materials*.
- [19]. Ji R, Zheng Y, Zou Z, et al. Utilization of mineral wool waste and waste glass for synthesis of foam glass at low temperature[J]. *Construction and Building Materials*, 2019, 215: 623-632.
- [20]. Shao Y , Lefort T , Moras S , et al. Studies on Concrete Containing Ground Waste Glass[J]. *Cement and Concrete Research*, 2000, 30(1):91-100.
- [21]. Chapelle L, Lyckegaard A, Kusano Y, et al. Determination of the fibre orientation distribution of a mineral wool network and prediction of its transverse stiffness using X-ray tomography[J]. *Journal of Materials Science*, 2018, 53(9):6390-6402.

-
- [22]. Väntsi O, Kärki T. Mineral wool waste in Europe: a review of mineral wool waste quantity, quality, and current recycling methods[J]. *Journal of Material Cycles and Waste Management*, 2014, 16(1): 62-72
- [23]. Väntsi O, Kärki T. Environmental assessment of recycled mineral wool and polypropylene utilized in wood polymer composites[J]. *Resources, Conservation and Recycling*, 2015, 104:38-48
- [24]. Kubiliute R , Kaminskas R , Kazlauskaitė A . Mineral wool production waste as an additive for Portland cement[J]. *Cement and Concrete Composites*, 2018, 88:130-138.
- [25]. Gao H T, Liu X H, Chen J Q, et al. Preparation of glass-ceramics with low density and high strength using blast furnace slag, glass fiber and water glass[J]. *Ceramics International*, 2017, 44(6):S0272884217329383
- [26]. Li Z , Luo Z , Li X , et al. Preparation and characterization of glass–ceramic foams with waste quartz sand and coal gangue in different proportions[J]. *Journal of Porous Materials*, 2016, 23(1):231-238.
- [27]. Lin K L, Lee T C, Hwang C L. Effects of sintering temperature on the characteristics of solar panel waste glass in the production of ceramic tiles[J]. *Journal of Material Cycles & Waste Management*, 2015, 17(1):194-200.
- [28]. Hong J M , Lin B , Jiang J S , et al. Synthesis of pore-expanded mesoporous materials using waste quartz sand and the adsorption effects of methylene blue[J]. *Journal of Industrial and Engineering Chemistry*, 2014, 20(5):3667-3671.
- [29]. Zhuo L, Luo Z, Li X, et al. Preparation and characterization of glass–ceramic foams with waste quartz sand and coal gangue in different proportions[J]. *Journal of Porous Materials*, 2016, 23(1):231-238.

-
- [30]. J. García-Ten, A. Saburit, E. Bernardo, P. Colombo, Development of lightweight porcelain stoneware tiles using foaming agents, *Journal of the European Ceramic Society*, 32 (2012) 745-752.
- [31]. S. Abbasi, S.M. Mirkazemi, A. Ziaee, M.S. Heydari, The effects of Fe₂O₃ and Co₃O₄ on microstructure and properties of foam glass from soda lime waste glasses, *Glass Physics & Chemistry*, 40 (2014) 173-179.
- [32]. Bontempi E. A new approach for evaluating the sustainability of raw materials substitution based on embodied energy and the CO₂ footprint[J]. *Journal of Cleaner Production*, 2017, 162.
- [33]. Vilcekova, Silvia, et al. "Comparison of environmental and energy performance of exterior walls." *Energy Procedia* 78 (2015): 231-236.
- [34]. Chen, Jiajian, et al. "Use of Quartz Sand to Produce Low Embodied Energy and Carbon Footprint Plaster." *Journal of Sustainable Architecture and Civil Engineering* 21.4 (2017): 75-81.
- [35]. Kirsch, B., et al. "Comparison of the embodied energy of a grinding wheel and an end mill." *Procedia CIRP* 15 (2014): 74-79.
- [36]. Hammond, Geoff, et al. *Inventory of carbon & energy: ICE*. Vol. 5. Bath: Sustainable Energy Research Team, Department of Mechanical Engineering, University of Bath, 2008.
- [37]. Dissanayake, D. M. K. W., C. Jayasinghe, and M. T. R. Jayasinghe. "A comparative embodied energy analysis of a house with recycled expanded polystyrene (EPS) based foam concrete wall panels." *Energy and Buildings* 135 (2017): 85-94.

Table and Figure Captions

Table 1: The chemical compositions of raw materials (wt.%)

Table 2: Main raw materials compositions of green samples (wt.%)

Table 3: the embodied energy and CO₂ footprint values of the materials involved

Figure 1: XRD pattern of raw materials

Figure 2: Variation of bulk density and a sectional view of base part samples without SiC at 1200°C

Figure 3: Variation of bulk density, a sectional view picture and SEM of insulation part samples with 2wt.% SiC at 1200°C

Figure 4: Variation of bulk density of sintered samples B3 and I3 at different temperatures

Figure 5: Bulk density variation of samples I3 with the different foaming agent

Figure 6: Bulk density variation of samples I3 with different sodium phosphate

Figure 7: The cross-sectional microstructure of samples I3 with different sodium phosphate (a) 0wt.%, (b) 1wt.%, (c) 2wt.%, (d) 3wt.%, (e)4 wt.%

Figure 8: The green sample and the sintered sample of the integrated envelope with both parts B3/I3

Figure 9: SEM image of the sectional view for this integrated envelope

Figure 10: The building model for evaluating the energy performance of the integrated envelope

Figure 11: Annual and monthly energy use for different building envelopes